PERINTIS
Persatuan Saintis Muslim Malaysia

PERINTIS eJournal
Vol. 15, No. 2, Dec 2025, pp. 37-46
e-ISSN: 2232-0725, DOI: 10.5281/zenodo.1808125

The Noise Reduction Algorithm for Star Detection

Anis Hannani Razaman, Yasser Asrul Ahmad, Teddy Surya Gunawan, Othman Omran Khalifa, Norazlina Saidin

Department of Electrical and Computer Engineering, Kulliyyah of Engineering, International Islamic University Malaysia, Jalan Gombak, 53100 Kuala Lumpur, Malaysia

Corresponding author: yasser@iium.edu.my
https://doi.org/10.5281/zenodo.1808125
Received 10 30, 2025
Revised 12 18, 2025
Accepted 12 29, 2025

ABSTRACT

Accurate star detection plays a critical role in star sensors for spacecraft attitude determination. However, various sources of noise such as cosmic radiation and sensor imperfections can degrade the accuracy of star centroid estimation. This paper presents a noise reduction algorithm that enhances the detection of star blobs in noisy star images. The proposed method integrates feature extraction through differential smoothing with adaptive thresholding techniques to effectively separate true star signals from background noise. To validate the algorithm, synthetic star images with different noise levels were tested. The results show that the proposed algorithm consistently detects all 20 target stars, achieving high detection accuracy even under severe noise conditions, outperforming conventional Laplacian of Gaussian (LoG) and Difference of Gaussian (DoG) approaches. This improvement in denoising leads to more precise centroid extraction, contributing to more reliable star sensor performance for space navigation applications.

Keywords: Star detection; noise reduction; centroiding algorithm; adaptive thresholding; space navigation.

1.0 INTRODUCTION

Star sensors play a crucial role in spacecraft navigation. Unlike celestial bodies such as the Moon and Sun, which provide limited reference points, stars offer an abundance of fixed positions, making them highly advantageous for space navigation. Star sensors detect stars, calculate their centroids, identify them, and determine the orientation and position of spacecraft or satellites. However, the brightness of stars can cause a large spread, obstructing detection [1]. It is essential to consider algorithms that can operate effectively under the harsh conditions of space, where bright solar reflections and cosmic radiation introduce noise into star images. One of the critical operations in star sensors is centroiding, which involves; the threshold segmentation to remove background noise, and centroid extraction to determine precise star locations. The objective of this paper is to study and evaluate noise reduction algorithms that enhance star detection for more accurate centroiding. In addition, we aim to develop a new algorithm that improves detection accuracy while maintaining lower computational complexity, based on insights from existing studies. By advancing denoising techniques, the accuracy of star centroid calculations can be optimized, thereby contributing to improved spacecraft navigation performance.

2.0 LITERATURE REVIEW

The space environment introduces several challenges that can interfere with reliable star detection and centroiding. Due to the lack of atmosphere, there is no scattering medium to diffuse sunlight, resulting in extremely harsh illumination contrasts, which then result to a low SNR environment. A low SNR directly affects centroiding performance by reducing star visibility, increasing false detections, and degrading positional accuracy [2]. As noted, star trackers provide greater accuracy than other attitude sensors like magnetometers, gyroscopes, sun sensors, and earth horizon sensors [3]. Two main types of imaging sensors are typically considered for star trackers: complementary metal-oxide semiconductor (CMOS) and charge-coupled device (CCD) [4], [5]. Active Pixel Sensor (APS) CMOS technology is especially suited for space missions, as it offers high integration, better resistance to radiation, lower power use, and lower cost compared to CCDs, making it ideal for power-constrained lunar missions [6].Two fundamental techniques used in image-based star detection are segmentation and centroiding. Thresholding is a segmentation method that separates star regions from the background by comparing pixel intensities to a set threshold. Pixels above the threshold are identified as stars, while lower ones are considered noise [7], [8]. This technique is commonly used for big bright object elimination such as moon and planets in the star maps [9].

A study evaluating seven thresholding algorithms; Bernsen, Otsu, Tsai, Niblack, Kittler-Illingworth, iterative thresholding, and improved iterative thresholding [10]. Bernsen's method excels with perfect true detection number (TDN) of 11/11 for image A across all 10 noise scenarios, the improved iterative method achieves acceptable TDN wchich is 94/94 for image C basics and up to 95 in mixed noise, outperforming the standard iterative (5/10 correct per image set) but faltering in 3-4 noise combinations with FDN rising to 760. Classical methods like Otsu and Niblack suffer high FDN. Otsu at 189-42053 false detections in image C noisy cases and rendering them unreliable beyond Poisson/multiplicative noise. Overall, Bernsen yields 10/10 correct detections for images A/B and 6/10 for C, confirming superior noise robustness among seven tested thresholding algorithms. However, o verreliance on TDN/FDN ignores centroiding accuracy post-detection, a critical downstream step, and simulated images (256x256 to 1024x1024) fail to represent high-FOV real trackers or dynamic distortions like motion blur.

Another technique, Binary Large Object (BLOB) detection is used to extract star images by identifying star-like objects in the captured images [11]. A comparative study from of four blob detection techniques; Laplacian of Gaussian (LoG), Difference of Gaussian (DoG), Determinant of Hessian (DoH) [12]. The results show that LoG and DoG detect a larger number of blobs, with LoG achieving the highest detection count (1,366 blobs), whereas DoH primarily detects larger blobs but with fewer detections (777 blobs). In addition, DoH produces the largest average blob size with greater size variation, while DoG records the shortest detection time at 4.27 seconds. The DoG method detects blobs by subtracting two Gaussian-blurred versions of an image with different standard deviations. This operation highlights intensity variations corresponding to blob-like structures while suppressing slow background changes [13], [14]. Meanwhile, LoG method first smooths the image using a Gaussian filter and then applies a Laplacian operator to identify regions of rapid intensity change [15]. Star candidates are detected at zero-crossings of the filtered image, which correspond to blob centers. The DoH method, which perfomed the best in this study, detects blobs by analyzing the second-order intensity derivatives using the Hessian matrix [16], [17]. It responds strongly to regions with pronounced curvature, allowing it to identify larger and more prominent star blobs. Though simple and efficient, its accuracy depends heavily on choosing the right threshold, as poor lighting or sensor noise can cause errors.

After detection, centroiding calculates the precise star location using the intensity-weighted average of pixel positions, achieving sub-pixel accuracy [18], [19]. This involves computing the

intensity-weighted average of pixel positions within a star region, resulting in a sub-pixel level estimate of the star's centre. This step is critical for applications like spacecraft attitude control, where small errors can impact orientation [2], [11], [20]. Accurate centroiding must account for noise, pixel quantization, and optical distortion.

3.0 METHODOLOGY

The proposed algorithm focuses on enhancing star detection by reducing noise interference, ensuring more accurate centroiding and identification of stars. As shown in Figure 1 is the proposed block diagram of the algorithm.

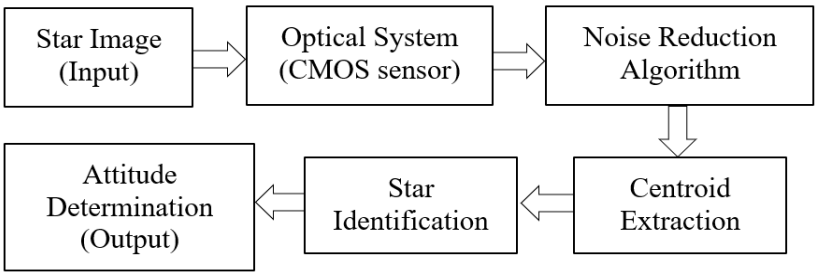

Figure 1: Block diagram of the proposed algorithm

The system starts with a star image captured using an optical system. The optical system used is a CMOS sensor, as discussed earlier, since the CMOS sensor performs better compared to other optical sensors. The captured image contains noise and distortion; therefore, the proposed noise reduction algorithm is applied to remove unnecessary corrupted pixels in the image. Next, the star centroid is calculated to extract the star coordinates, followed by star identification, which is then used to determine the spacecraft attitude.

In this study, the focus is placed on enhancing the noise reduction algorithm within the star sensor processing pipeline. Although the full system includes stages from capturing the star image to determining the spacecraft's direction, this paper only looks at the part where we reduce noise caused by things like radiation and surface reflection. We test how well our method works by using centroid extraction to check how accurate the detected star positions are compared to known star data.

The algorithm begins with an initial feature extraction step that isolates star candidates from the background. To prove that the proposed algorithm is ribust to noises, we simulate Gaussian noise and added it into the star images. Gaussian noise is commonly used to simulate sensor noise in optical devices and is mathematically characterised by its probability density function [21].

$$p(x) = \frac{1}{\sqrt{2\pi\sigma^2}} exp\left(-\frac{(x-\mu)^2}{2\sigma^2}\right) \quad (1)$$

The parameters used are: $mean, \mu = 0$, $variance, \sigma^2 = 0.01$. For each pixel $I(x, y)$ [22]:

$$I_{gaussian}(x, y) = I(x, y) + n_{gaussian}(x, y) \quad (2)$$

Where the noise term is drawn from Gaussian (normal) distribution:

$$n_{gaussian}(x, y) \sim N(0, 0.01) \quad (3)$$

So the noise spreads around zero, with strength controlled by the variance.

To refine this section, a differential smoothing step is applied, which enhances the distinction between true star signals and background variations by adjusting contrast dynamically based on local pixel neighbourhoods [23]. This ensures that star spots remain detectable even under strong gradients caused by reflections or radiation noise. Equation (4)-(6) is the derivation and modification from blob detection methods, discussed previously [11]. The image convolved with two Gaussian filters with different standard deviations σ_1 and σ_2, controlling the amount of smoothing. A larger σ smooths over larger areas. The image $I(x, y)$ is smoothed at both scales.

$$I_{\sigma_1}(x, y) = I(x, y) * G_{\sigma_1}(x, y), \quad (4)$$

$$I_{\sigma_2}(x, y) = I(x, y) * G_{\sigma_2}(x, y) \quad (5)$$

Subtract the smoothed images to highlight intensity changes, as shown in equation (6). Positive values of $I_{blob}(x, y)$ indicate areas of increased intensity (bright blobs), meanwhile, the negative values indicate areas of reduced intensity. Near-zero values represent flat regions (background).

$$I_{blob}(x, y) = I_{\sigma_1}(x, y) - I_{\sigma_2}(x, y) \quad (6)$$

Following feature extraction, the thresholding technique is introduced, allowing for adaptive segmentation based on intensity variations across the image. The image is divided into small windows centred at each pixel (x, y). Then, compute the local mean intensity $M(x, y)$ in equation (7), and the threshold value in equation (8) [24], [25]:

$$L_{mean}(x, y) = \frac{1}{N} \sum_{(i,j)\epsilon W} I(i, j), \quad (7)$$

$$I_{output}(x, y) = \frac{L_{max} + L_{min}}{2} \quad (8)$$

The difference between the blob (represent as 1) and the background (represent as 0) can be decided:

$$I_{output}(x, y) = \begin{cases} 1, & if\ I_{DoG}(x, y) \geq L_{mean}(x, y) \\ 0, & otherwise \end{cases} \quad (9)$$

If the intensity of the original image at pixel (x, y), denoted as $I(x, y)$, is greater than or equal to the calculated threshold value $T(x, y)$, then that pixel is classified as belonging to a blob (which could be a star) and is assigned a binary value of 1. Otherwise, if the intensity $I(x, y)$ is less than the threshold value $T(x, y)$, the pixel is classified as background and assigned a binary value of 0.

Finally, the performance of the proposed noise reduction method will be compared with standard LoG and DoG techniques to evaluate its effectiveness in improving star detection accuracy under challenging conditions. The detection accuracy can be calculated with equation (10):

$$Detection\ Accuracy(\%) = \frac{\min\left(N_{detected}, N_{actual}\right)}{N_{actual}} \quad (10)$$

The performance will be evaluated using the synthetic star images with different noise levels and star distributions, as shown in Figure 2 (a) and (b).

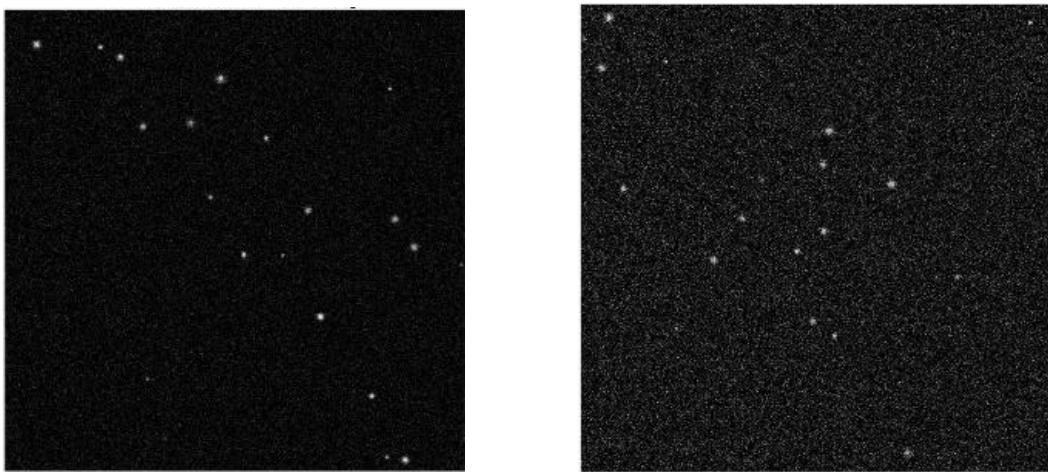

(a) (b)

Figure 2: Synthetic star images (a) 0.01 noise level (b) 0.05 noise level

Although the star positions vary between the images, this does not affect the testing process, as each image is processed independently. The purpose of this test is to validate whether the proposed algorithm can effectively reduce noise and enhance star features under varying conditions. The variation in star location across images does not interfere with the validation, as the focus is on the clarity and accuracy of the extracted star centroids after noise reduction.

4.0 RESULTS AND DISCUSSION

We collected data of total stars detected in synthetic images under different noise levels. We evaluate the result by comparing the detection performance between three algorithm techniques: LoG, DoG and proposed noise reduction algorithm.

4.1 Laplacian of Gaussian (LoG)

Firstly, we tested the LoG algorithm on the synthetic image of 20 stars with 0.01 noise level. Figure 3 (a) and (b) shows the algorithm can detect some of the stars but mistook some of the noise as the star.

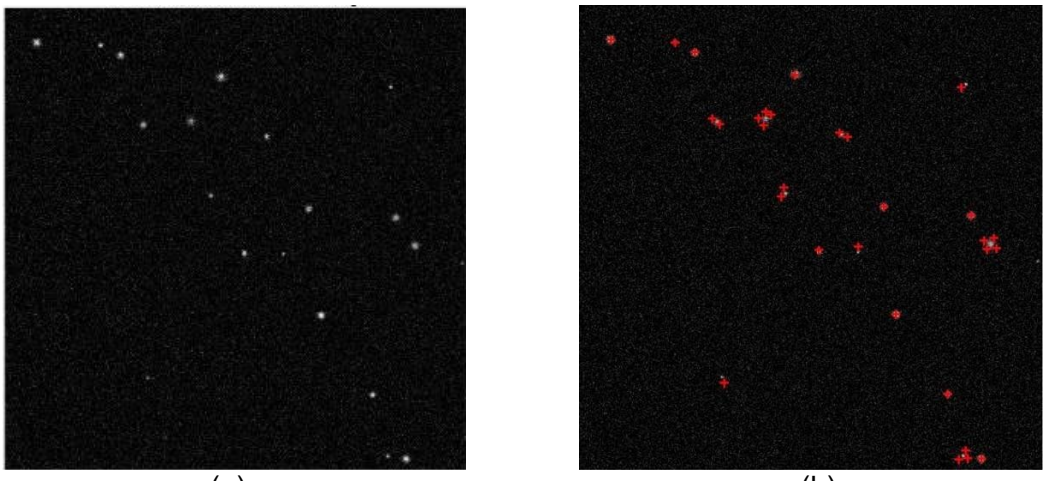

(a) (b)

Figure 3: Star detection (a) Synthetic image of 0.01 noise level (b) Star detected using LoG method

For the noise level of 0.05, as shown in Figure 4 (a) and (b), the algorithm incorrectly identified numerous noise artifacts as stars, resulting in a significant number of false detections from the original 20 synthetic star blobs.

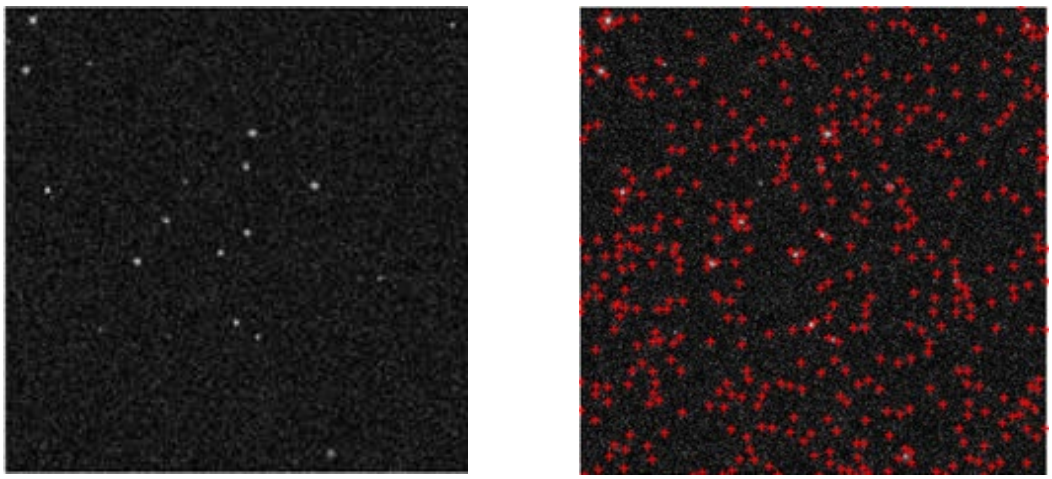

(a) (b)

Figure 4 : Star detection (a) Synthetic image of 0.05 noise level (b) Star detected using LoG method

4.2 Difference of Gaussian (DoG)

Hence, we changed the LoG method by using DoG technique. Figures 5 (a) and (b) show that the technique successfully detected all the 20 stars within 0.01 noise level.

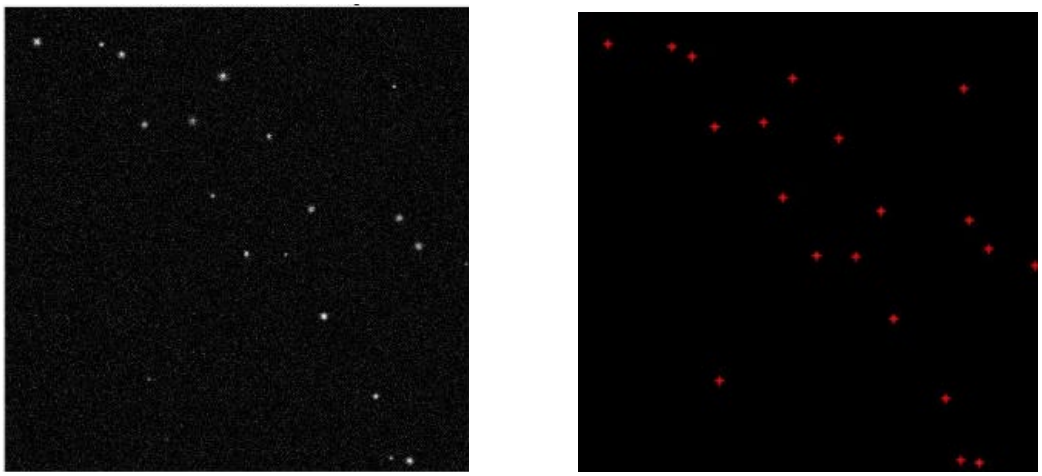

(a) (b)

Figure 5: Star detection (a) Synthetic image of 0.01 noise level (b) Star detected using DoG method

However, after we increased the noise level to 0.05, it detected around 26 blobs as the stars, shown in Figures 6 (a) and (b). A similar issue occurred with the LoG technique at the noise level of 0.01, where it indicates that a significant number of noise points were misinterpreted as stars.

In the DoG method, different standard deviations (σ) affect detection accuracy. A small σ captures fine details but amplifies noise, while a large σ smooths the image, potentially losing faint stars. The right σ combination enhances contrast, suppresses noise, and ensures accurate star detection without false positives or missing features.

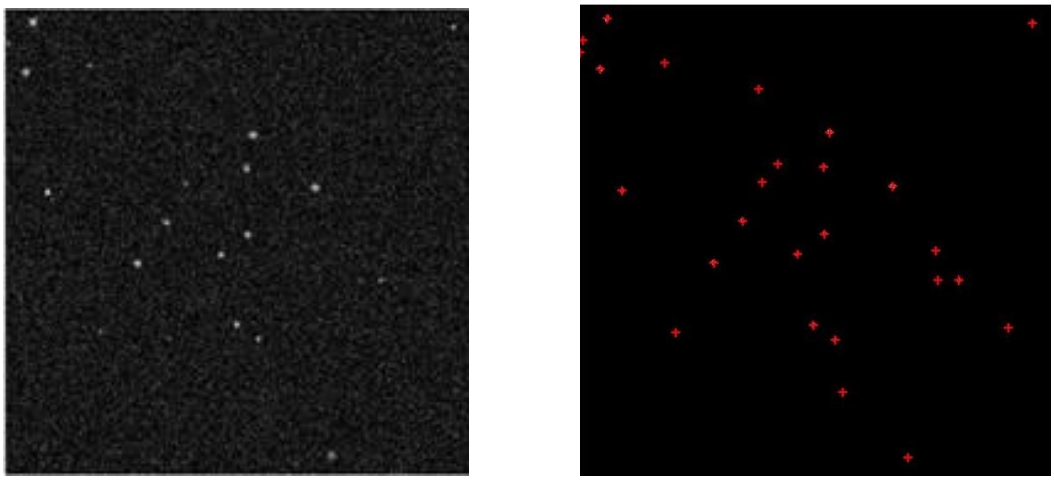

(a) (b)

Figure 6: Star detection (a) Synthetic image of 0.05 noise level (b) Star detected using DoG method

4.3 Proposed Algorithm

To enhance the blob detection accuracy within the 0.05 noise level, we apply our proposed algorithm where it integrates the feature extraction and thresholding techniques. As shown in Figure 7 (a) and (b), the 20 stars were successfully detected.

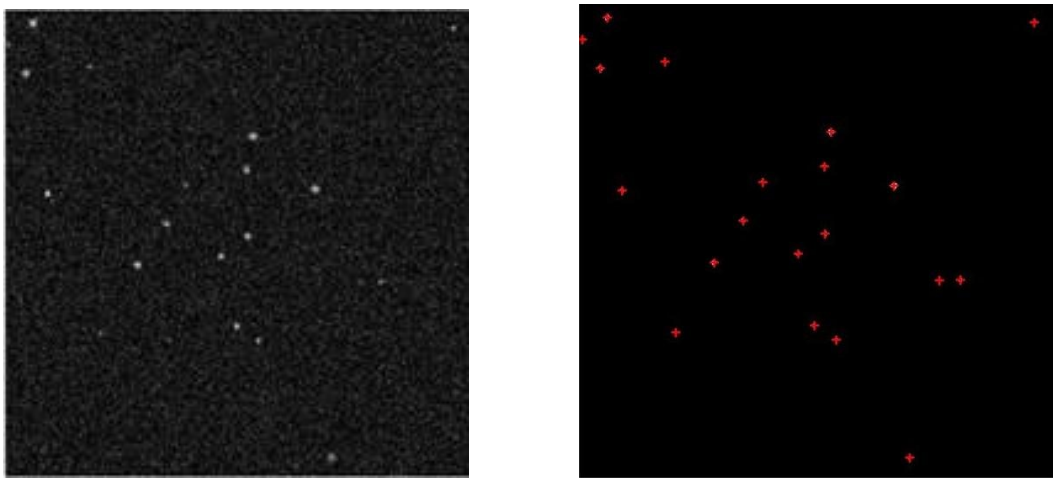

(a) (b)

Figure 7: Synthetic image of 0.05 noise level (b) Star detected using proposed method.

4.4 Comparison Summary

Table 1 presents the comparison of star detection performance under two different noise levels (0.01 and 0.05) using three algorithms: Laplacian of Gaussian (LoG), Difference of Gaussian (DoG), and the proposed algorithm.

Table 1: Table of Summary

Algorithm	Laplacian of Gaussian (LoG		Difference of Gaussian (DoG)		Proposed Algorithm	
Noise Level	0.01	0.05	0.01	0.05	0.01	0.05
Star Detected	29	~600	20	26	20	20
Detection Accuracy (%)	68.9	3.3	91.1	76.9	98.8	98.3

At a low noise level of 0.01, LoG detected 29 blobs, resulting in a detection accuracy of 68.9%, indicating a considerable number of false positives. DoG performed better with 20 detections and an accuracy of 0.911, while the proposed algorithm achieved the highest accuracy of 98.8% by correctly detecting all 20 stars with minimal false detections. Under a higher noise level of 0.05, LoG showed significant performance degradation, detecting around 600 blobs with a very low accuracy of 3.30% due to misclassification of noise as stars. DoG detected 26 blobs with an accuracy of 76.9%, while the proposed algorithm remained robust, accurately detecting all 20 stars with an accuracy of 98.3%. These results demonstrate the effectiveness and resilience of the proposed method in maintaining high detection accuracy even under challenging noise conditions.

5.0 CONCLUSION AND FUTURE WORKS

To identify star regions effectively amidst noise, we compared two blob detection methods: the Laplacian of Gaussian (LoG) and the Difference of Gaussian (DoG). Both approaches were evaluated for their ability to enhance star detection accuracy, particularly under conditions with varying levels of noise and interference. After an initial analysis, we determined that the DoG method performed better due to its improved precision in isolating star features while reducing noise. Consequently, we applied our proposed algorithm to further enhance robustness and ensure reliable detection in diverse noisy environments. From the initial testing with the synthetic images, it is proven that the integration of differential smoothing and adaptive thresholding methods performed the best for detecting all 20 stars in the noisy image. Additionally, we conclude that the gaussian kernel need to be carefully considered to optimize detection accuracy. It is also crucial to determine a suitable threshold value to further enhance the star detection and centroiding algorithm, ensuring more precise and reliable results.

The proposed research aims to achieve several key outcomes in the future. First, the performance of the centroiding algorithm will be enhanced to optimize its speed and reduce runtime, ensuring efficient star detection and tracking. Second, the developed algorithm will be tested using synthetic and existing star images that contain different types of noise to simulate real-world conditions such as: Gaussian noise, Poisson noise, Speckle noise and Salt-and-Pepper noise. Lastly, the algorithm will be validated under real-world conditions by testing it in a night sky environment and under varying celestial conditions using a star sensor integrated camera and an image sensor. This practical implementation will demonstrate the robustness and adaptability of the algorithm in diverse scenarios.

ACKNOWLEDGEMENT

This research was fully funded by Malaysia's Ministry of Higher Education (MoHE) Fundamental Research Grant Scheme (FRGS) code number FRGS/1/2024/TK07/UIAM/02/1 and KHAIR Award by Center for Postgraduate Studies (CPS) IIUM.

REFERENCES

[1] T. I. Liaudat, J.-L. Starck, and M. Kilbinger, “Point spread function modelling for astronomical telescopes: a review focused on weak gravitational lensing studies,” *Frontiers in Astronomy and Space Sciences*, vol. 10, Oct. 2023, doi: 10.3389/fspas.2023.1158213.

[2] C. C. Liebe, “Accuracy performance of star trackers - a tutorial,” *IEEE Trans Aerosp Electron Syst*, vol. 38, no. 2, pp. 587–599, Apr. 2002, doi: 10.1109/TAES.2002.1008988.

[3] X. Qian, H. Yu, and S. Chen, “A Global-Shutter Centroiding Measurement CMOS Image Sensor With Star Region SNR Improvement for Star Trackers,” *IEEE Transactions on Circuits and Systems for Video Technology*, vol. 26, no. 8, pp. 1555–1562, 2016, doi: 10.1109/TCSVT.2015.2469091.

[4] E. R. Fossum, “CMOS Image Sensors and the Quanta Image Sensor,” in *2018 International Conference on Optical MEMS and Nanophotonics (OMN)*, 2018, pp. 1–5. doi: 10.1109/OMN.2018.8454568.

[5] E. R. Fossum and D. B. Hondongwa, “A Review of the Pinned Photodiode for CCD and CMOS Image Sensors,” *IEEE Journal of the Electron Devices Society*, vol. 2, no. 3, pp. 33–43, 2014, doi: 10.1109/JEDS.2014.2306412.

[6] F. Xing, Y. Dong, Z. You, and Q. Zhou, “APS star tracker and attitude estimation,” in *2006 1st International Symposium on Systems and Control in Aerospace and Astronautics*, 2006, pp. 5 pp. – 38. doi: 10.1109/ISSCAA.2006.1627697.

[7] R. C. Gonzalez and R. E. Woods, *Digital Image Processing, 4th ed.*, 4th ed. Pearson, 2018.

[8] J. Rogowska, “Overview and Fundamentals of Medical Image Segmentation,” *Handbook of Medical Imaging*, pp. 69–85, 2000, doi: 10.1016/B978-012077790-7/50009-6.

[9] Z. Mahi, M. S. Karoui, and M. Keche, “A Non-Stellar Big Bright Object Elimination and Star Centroid Extraction Algorithm for Star Tracker,” in *2024 IEEE Mediterranean and Middle-East Geoscience and Remote Sensing Symposium (M2GARSS)*, 2024, pp. 1–5. doi: 10.1109/M2GARSS57310.2024.10537475.

[10] Z. Mahi and M. S. Karoui, “A Comparative Study of Star Detection Methods for a Satellite-Onboard Star Tracker,” in *2019 International Conference on Advanced Electrical Engineering (ICAEE)*, 2019, pp. 1–6. doi: 10.1109/ICAEE47123.2019.9015160.

[11] C. Chen, Q. Chen, C. Gao, N. Zhang, X. Wang, and Y. Zhai, “Method of Blob detection based on radon transform,” in *2018 Chinese Control And Decision Conference (CCDC)*, 2018, pp. 5762–5767. doi: 10.1109/CCDC.2018.8408138.

[12] S. S, M. R, M. D, and M. A, “Performance Evaluation of Blob Detection Techniques Using Image Processing,” in *2024 4th International Conference on Sustainable Expert Systems (ICSES)*, IEEE, Oct. 2024, pp. 1101–1106. doi: 10.1109/ICSES63445.2024.10763362.

[13] C.-H. Liu, M.-F. Zhang, W.-J. Zhang, X. Hu, S.-H. Peng, and C.-R. Zou, “Automatic nodule location based on a modified Difference of Gaussian detector,” in *2015 8th International Congress on Image and Signal Processing (CISP)*, IEEE, Oct. 2015, pp. 428–432. doi: 10.1109/CISP.2015.7407918.

[14] T. Leelawattananon and S. Chittayasothorn, “Electronic Parts Counting in Physics Laboratory Using Difference of Gaussians Edge Extraction,” in *2024 12th International Conference on Information and Education Technology (ICIET)*, IEEE, Mar. 2024, pp. 338–342. doi: 10.1109/ICIET60671.2024.10542805.

[15] T.-H. Lee *et al.*, “Laplacian of Gaussian Based on Color Constancy Algorithm for Surrounding Image Stitching Application,” in *2022 IEEE International Conference on Consumer Electronics - Taiwan*, IEEE, Jul. 2022, pp. 287–288. doi: 10.1109/ICCE-Taiwan55306.2022.9869055.

[16] M. E. Aydin and M. Ergut, “Hessian determinants of composite functions with applications for production functions in economics,” *Kragujevac Journal of Mathematics*, vol. 38, no. 2, pp. 259–268, 2014, doi: 10.5937/KgJMath1402259A.
[17] M. Carlsson, V. Nikitin, and H. Wendt, “Phase retrieval using the Hessian operator,” in *2025 IEEE Statistical Signal Processing Workshop (SSP)*, IEEE, Jun. 2025, pp. 46–50. doi: 10.1109/SSP64130.2025.11073275.
[18] J. R. Janesick, *Scientific Charge-Coupled Devices*. SPIE, 2001. doi: 10.1117/3.374903.
[19] W. N. J. H. W. Yussof, M. Man, R. Umar, A. N. Zulkeflee, E. A. Awalludin, and N. Ahmad, “Enhancing Moon Crescent Visibility Using Contrast-Limited Adaptive Histogram Equalization and Bilateral Filtering Techniques,” *Journal of Telecommunictions and Information Technology*, vol. 1, no. 2022, pp. 3–13, Mar. 2022, doi: 10.26636/jtit.2022.155721.
[20] Wayne Niblack, *An Introduction to Digital Image Processing*. Strandberg Publishing Company, Denmark, 1985.
[21] J. Sauvola and M. Pietikäinen, “Adaptive document image binarization,” *Pattern Recognit*, vol. 33, no. 2, pp. 225–236, Feb. 2000, doi: 10.1016/S0031-3203(99)00055-2.